Space Weather

RESEARCH ARTICLE
10.1029/2020SW002477

Key Points:
- The radiation belt responds to both CME- and CIR-driven geomagnetic storms in a consistent and repeatable way
- Two storm phases, dominated by loss and then acceleration, have strong albeit different correlations to solar wind and geomagnetic drivers
- These results provide an overarching framework that provides a coherent description of storm time radiation belt dynamics

Supporting Information:
- Supporting Information S1

Correspondence to:
K. R. Murphy,
krmurphy@umd.edu

Citation:
Murphy, K. R., Mann, I. R., Sibeck, D. G., Rae, I. J., Watt, C. E. J., Ozeke, L. G., et al. (2020). A framework for understanding and quantifying the loss and acceleration of relativistic electrons in the outer radiation belt during geomagnetic storms. *Space Weather*, *18*, e2020SW002477. https://doi.org/10.1029/2020SW002477

Received 13 FEB 2020
Accepted 22 MAR 2020
Accepted article online 17 APR 2020

A Framework for Understanding and Quantifying the Loss and Acceleration of Relativistic Electrons in the Outer Radiation Belt During Geomagnetic Storms

Kyle R. Murphy[1,2], Ian R. Mann[2,3], David G. Sibeck[2], I. Jonathan Rae[4], C.E.J. Watt[5], Louis G. Ozeke[3], Shri G. Kanekal[2], and Daniel N. Baker[6]

[1]Department of Astronomy, University of Maryland, College Park, MD, USA, [2]NASA Goddard Space Flight Centre Code 674, Greenbelt, MD, USA, [3]Department of Physics, University of Alberta, Edmonton, Alberta, Canada, [4]Department of Space and Climate Physics, Mullard Space Science Laboratory, University College London, London, UK, [5]Department of Meteorology, University of Reading, Reading, UK, [6]Laboratory for Atmospheric and Space Physics, University of Colorado Boulder, Boulder, CO, USA

Abstract We present detailed analysis of the global relativistic electron dynamics as measured by total radiation belt content (RBC) during coronal mass ejection (CME) and corotating interaction region (CIR)-driven geomagnetic storms. Recent work has demonstrated that the response of the outer radiation belt is consistent and repeatable during geomagnetic storms. Here we build on this work to show that radiation belt dynamics can be divided into two sequential phases, which have different solar wind dependencies and which when analyzed separately reveal that the radiation belt responds more predictably than if the overall storm response is analyzed as a whole. In terms of RBC, in every storm we analyzed, a phase dominated by loss is followed by a phase dominated by acceleration. Analysis of the RBC during each of these phases demonstrates that they both respond coherently to solar wind and magnetospheric driving. However, the response is independent of whether the storm response is associated with either a CME or CIR. Our analysis shows that during the initial phase, radiation belt loss is organized by the location of the magnetopause and the strength of Dst and ultralow frequency wave power. During the second phase, radiation belt enhancements are well organized by the amplitude of ultralow frequency waves, the auroral electroject index, and solar wind energy input. Overall, our results demonstrate that storm time dynamics of the RBC is repeatable and well characterized by solar wind and geomagnetic driving, albeit with different dependencies during the two phases of a storm.

1. Introduction

During intervals of enhanced solar wind driving, such as following the impact of interplanetary coronal mass ejections (CMEs) or corotating interaction regions (CIRs), the relativistic electron fluxes within the outer Van Allen radiation belt are extremely variable. These dynamic periods often lead to geomagnetic storms during which the flux of relativistic electrons can change by several orders of magnitude. Despite recent advances in understanding the nature of competing radiation belt acceleration and loss processes during geomagnetic storms (e.g., Kanekal et al., 2016; Li et al., 2014; Mann et al., 2016; Olifer et al., 2018; Reeves et al., 2013; Su et al., 2015; Tu et al., 2014), modeling and forecasting geomagnetic storms and the variation in relativistic electron flux in the outer Van Allen radiation belt have remained extremely challenging. This is in part because geomagnetic storms can produce a range of responses in the flux of outer radiation belt electrons including a net enhancement, a net depletion, or no net change (Anderson et al., 2015; Reeves et al., 2003). Moreover, although the solar wind drivers are well defined from upstream spacecraft observations, previous analyses of the overall change in outer radiation belt flux resulting from geomagnetic storms have shown that the prestorm and poststorm fluxes of relativistic electrons are highly uncorrelated and independent of storm strength (Anderson et al., 2015; Reeves et al., 2003).

Despite the inherent complexity in the response of the flux of outer radiation belt electrons, recent studies have demonstrated that the dynamics of outer radiation belt can be quite well characterized when studied separately as a function of storm phase (e.g., Murphy et al., 2018), and the response assessed in terms of

electron energy (e.g., Jaynes et al., 2015; Murphy et al., 2018; Turner et al., 2015), prevailing solar wind conditions (e.g., O'Brien et al., 2001), and solar wind driver (e.g., Bingham et al., 2018; Hietala et al., 2014; Kilpua et al., 2015; Miyoshi et al., 2013; Morley et al., 2010; Yuan & Zong, 2012) as discussed below.

In a statistical study of total radiation belt content (RBC; an estimate of the total number of electron in the outer radiation belt at a fixed first adiabatic invariant) derived from Van Allen Probes phase space density during 73 geomagnetic storms, Murphy et al. (2018) showed that the response of the seed (hundreds of keV), relativistic (~1 MeV), and ultrarelativistic (~2.5 MeV) electron radiation belt populations during the main phase and recovery phase of geomagnetic storms is well ordered. During geomagnetic storms, the radiation belt seed population undergoes a strong and nearly immediate enhancement following the storm commencement, which continues through the main phase (see also Turner et al., 2015). At higher energies, the relativistic and ultrarelativistic populations are characterized by a net loss of electrons during the main phase followed by a period of net rapid acceleration during the storm recovery phase following the enhancement in the seed population (Murphy et al., 2018). In a study of an extended period of geomagnetic activity between August–September 2014, Jaynes et al. (2015) demonstrated that the behavior of the radiation belt seed population appeared to be closely related to radiation belt enhancements in the relativistic and ultrarelativistic populations. Active geomagnetic conditions with sustained substorm activity lead to enhancements in low energy seed electrons and subsequently the relativistic and ultrarelativistic electron populations, whereas periods with limited substorm activity and a lower flux of lower-energy seed electrons resulted in a dearth of relativistic electrons in the outer radiation belt (Baker et al., 1998; Bingham et al., 2018; Jaynes et al., 2015). These results are qualitatively similar to those found by Murphy et al. (2018).

Several studies have also demonstrated that radiation belt depletions and enhancements can be associated with specific large-scale solar wind features and characteristic interplanetary magnetic field (IMF) or solar wind drivers. With regard to radiation belt loss, Morley et al. (2010) showed that stream interfaces (SIs) were generally associated with electron loss or radiation belt dropouts. These authors attributed the observed losses to outward radial diffusion and magnetopause shadowing (e.g., Loto'aniu et al., 2010; Shprits et al., 2006; Turner et al., 2012a) and chorus-driven microbursts (e.g., O'Brien et al., 2004). Though these authors did not specifically study storm time radiation belt dynamics, Morley et al. (2010) did demonstrate that outer radiation belt electrons respond consistently to SIs. Kilpua et al. (2015) characterized the response of energetic electrons at geosynchronous orbit to large-scale solar wind drivers, including CMEs and CIRs as and their substructure (see Kilpua et al., 2015, for details). These authors found that radiation belt electron loss at high L-shells tended to dominate during SIs, similar to the results of Morley et al. (2010), as well as during the ejecta and sheath portions of an interplanetary CME (see also Hietala et al., 2014).

In a study of storm time electromagnetic ion cyclotron (EMIC) waves in the magnetosphere, Halford et al. (2010) found that the occurrence of EMIC waves peaked during the main phase of storms. These authors postulated that pitch angle scattering by EMIC waves could be an important radiation belt loss process during the main phase of storms (e.g., Meredith et al., 2003; Ukhorskiy et al., 2010); recent modeling work supports this (e.g., Shprits et al., 2013). For an excellent overview of radiation belt losses and dropouts, we direct the reader to Turner et al. (2012b).

Regarding radiation belt enhancements specifically, O'Brien et al. (2001) concluded that storm time enhancement of the outer radiation belt at geosynchronous orbit requires a period of sustained high-speed solar wind and enhanced ULF wave power in the inner-magnetosphere (see also Mathie & Mann, 2000, 2001). In a statistical study of CME- and CIR-driven storms and total RBC derived from SAMPEX observations, Yuan and Zong (2012) demonstrated that over the entire outer radiation belt, CME-driven storms are more effective than CIR-driven storms in accelerating radiation belt electrons. These authors also demonstrated that CME-driven storms are more effective at driving enhancement at lower L-shells, whereas at geosynchronous orbit, CIRs are more effective at driving enhancements (see also Miyoshi & Kataoka, 2005). Miyoshi and Kataoka (2005) attributed the radial differences in storm time electron enhancements observed in CME- and CIR-driven storms to solar cycle phase. During solar maximum, when the occurrence of CMEs peaks, the outer radiation belt moves inward to lower L-shells, and during the declining phase, when the occurrence of CIRs peaks, the outer radiation belt moves outward. Hence, these authors concluded that enhancements in radiation belt electrons are more likely to be observed closer to the Earth when driven by CMEs and further from the Earth when driven by CIRs, a simple function of the

ambient location of the outer radiation belt. Finally, in a statistical study of storm time radiation belt electron dynamics observed by the Van Allen Probes, Bingham et al. (2018) also found that CME-driven storms, on average, showed greater radiation belt electron enhancements compared to CIR-driven storms, consistent with Yuan and Zong (2012). These authors concluded that this difference was likely due to an earlier and deeper penetration of radiation belt seed electrons driven by enhanced convection and substorm activity during observed during CME-driven storms (Baker et al., 1998; Jaynes et al., 2015).

In this study we build on this extensive body of work by studying the dynamics of the outer radiation belt using the long-duration data set available from the SAMPEX spacecraft to help further understand the physical processes that control both loss and acceleration of relativistic electrons during geomagnetic storms. We investigate storm time radiation belt dynamics driven by CMEs and CIRs utilizing data from SAMPEX and the derived RBC index (Baker et al., 2004). Our analysis and framework combine aspects of both autoregressive and multiple regression techniques used to describe and forecast time-varying processes (e.g., Borovsky, 2014; Shumway & Stoffer, 2006) to quantify the processes controlling relativistic electron loss and acceleration through geomagnetic storms. The details of this analysis, including the calculation of the RBC index, the storm database used, and the storm time dynamics of the outer radiation belt revealed by the analysis, are presented in section 2. Section 3 provides a detailed discussion of the results presented in section 2 and presents our conclusions.

Overall, by separating each storm into two independent phases, an initial phase dominated by losses and a second dominated by enhancements, and quantifying the physical processes controlling radiation belt dynamics (based on the work described above), we demonstrate that the entire outer radiation belt responds consistently to solar wind and geomagnetic driving during geomagnetic storms. Significantly, we demonstrate that a large component of relativistic electron loss in the outer radiation belt during storms is consistent with the Dst effect and ULF wave-enhanced magnetopause shadowing. Storm time enhancements of relativistic electron fluxes in the outer radiation belt during storms have a strong contribution from solar wind energy input, substorms, and likely energization via ultralow frequency (ULF) and very low frequency (VLF) waves.

2. Data and Analysis

2.1. The RBC Index

The Solar Anomalous and Magnetospheric Particle Explorer (SAMPEX) is a low-Earth orbiting satellite designed to study cosmic rays, solar energetic particles, and magnetospheric electron precipitation at relativistic energies (see the review by Baker & Blake, 2012, and reference therein). Despite being designed to study electron precipitation, SAMPEX can also be used to study the dynamics of outer radiation belt electrons during geomagnetic storms, due to a strong coherence in outer radiation belt electrons, which exists as a function of altitude (when compared between two sets of observations) (Chen et al., 2016; Kanekal et al., 2001) or of electron pitch angle (when observed in situ with single point observations) (Murphy et al., 2018). Hence, even though low-Earth orbiting satellites observe the low pitch angle tail of the equatorial pitch angle distribution, they can still be used to study storm time radiation belt electron dynamics (Chen et al., 2016; Kanekal et al., 2001). As a radiation belt monitor, SAMPEX also has the capability to investigate outer radiation belt dynamics over an entire solar cycle (e.g., Baker & Blake, 2012).

In this study we use the Proton/Electron Telescope (Baker & Blake, 2012) onboard SAMPEX to derive a RBC index (Baker et al., 2004) and statistically characterize the temporal response of storm time relativistic electron dynamics during previously identified geomagnetic storms, which are described in detail below. The RBC index provides a means to reduce the dimensionality of the SAMPEX PET instrument data by removing relativistic electron dynamics as a function of L while still being able to characterize the temporal dynamics of the overall system including periods dominated by electron loss or acceleration (e.g., Murphy et al., 2018). In this study the RBC is calculated by integrating the daily averaged 1.5–6 MeV electron flux between McIllwain's $L = 2$ and $L = 8$ (as provided by CDAWeb and calculated from IGRF) stepped every 6 hr. This integration provides an estimate of the total number of electrons in the energy range 1.5–6 MeV between fixed inner and outer L-shell boundaries with a 6 hr cadence (cf. Baker et al., 2004; Yuan & Zong, 2012). Details of the calculation of the RBC can be found in Supporting Information S1 and in Baker et al. (2004). The RBC index is also provided in Supporting Information S2.

The advantage of the RBC index is that it reduces the dimensionality of the SAMPEX 1.5–6 MeV electron flux, which allows the dynamics of the outer radiation belt to be statistically analyzed over of the course of many storms (e.g., Baker et al., 2004; Forsyth et al., 2016; Murphy et al., 2018; Yuan & Zong, 2012). Though the RBC index is ideal for statistically characterizing storm time radiation belt dynamics, it is not without its limitations, as Baker et al. (2004) noted, physical processes in the outer radiation belt are both physically complex and can be spatially varied, which will affect any estimation of RBC. For example, two physical processes that affect the RBC derived here are the motion of the electron mirror point and adiabatic effects, both of which can act to artificially reduce the RBC index, especially during geomagnetic storms. These processes are also discussed further below.

During geomagnetic storms, the electron mirror point for certain pitch angles can move above low-altitude satellites such as SAMPEX, such that the satellite observes an apparent decrease in electron flux (Selesnick, 2006; Tu & Li, 2011), thus affecting any calculation of the RBC. However, in the presence of moderate pitch angle scattering, such as that observed during storms (Li et al., 2007), the loss cone rapidly refills limiting the effects of changing mirror points at low altitudes (Selesnick, 2006; Selesnick & Kanekal, 2009). Further, Chen et al. (2016) have shown a high coherence exists between equatorial and low-altitude observations of the outer radiation belt and have demonstrated the robustness of low-altitude observations in predicting equatorial radiation belt dynamics. Therefore, the effects of mirror point motion on the RBC index are expected to be limited.

As noted above and in the supporting information, since the RBC index is derived from electron flux as a function of L and across a fixed energy range, it is also susceptible to adiabatic changes during geomagnetic storms including those arising from the Dst effect. In this study, adiabatic changes in electron flux are partially mitigated by integrating over an extended range in L-shell such that any adiabatic changes in electron flux resulting from either the Dst effect or compressions of the magnetospheric magnetic field are still captured within the L-shell range which is integrated to create the RBC index. Kim et al. (2010) demonstrated that during storms, the change in L of equatorial electrons due to the Dst effect in the heart of the radiation belt ($L \sim 3.5$–4.5) is less 1 R_E. By integrating over fixed $L = [2, 8]$, the core of the radiation belt flux at 3–5 R_E (e.g., Yuan & Zong, 2012) is always included in the RBC derivation, even during such adiabatic changes. In addition, Morley et al. (2010) noted that the dynamics of electron flux during SIs as a function of L and L^* are qualitatively similar; thus, for the purpose of characterizing large-scale electron dynamics, the RBC index derived here is still able to characterize both electron loss and acceleration, without being significantly contaminated by those adiabatic and transient changes. Thus, while we could not completely exclude adiabatic effects in this study, through the choice of L domain we are able to mitigate them.

Despite the limitations, understanding how the absolute flux of relativistic electrons at fixed energies varies, regardless of adiabatic or nonadiabatic changes, remains important for satellite operations and for mitigating the effects on satellite infrastructure associated, for example, with deep dielectric charging (e.g., Horne et al., 2013; Schrijver et al., 2015).

2.2. Storm Database

In this study we use previously identified storms compiled from Denton et al. (2006), Kataoka and Miyoshi (2006), and Hutchinson et al. (2011) to study dynamics of the outer radiation belt as characterized by the RBC index during CME- and CIR-driven storms. The Denton et al. (2006) database contains 124 CIR driven storms between 1993 and 2005 that are selected based on prevailing solar wind conditions. Kataoka and Miyoshi (2006) identified isolated storms by a decrease in Dst below −100 nT and further characterized the predominant solar wind driver as either a CME or CIR related. Their list comprises 55 storms, 49 CME, and 6 CIRs driven storms. The Hutchinson et al. (2011) storm list contains 143 storms, 104 CME-driven storms, and 39 CIR-driven storms. Hutchinson et al. (2011) used the characteristic response of Sym-H to characterize geomagnetic storms; events were selected if they exhibited an initial phase (or sudden commencement), main phase, and recovery phase. The prevailing solar wind conditions were then used to further subdivide these events into CME- and CIR-driven storms. In each of these three storm lists, no geomagnetic storm is identified based on the dynamics of the outer radiation belt, and thus, there is no assumed a priori response of the outer radiation belt.

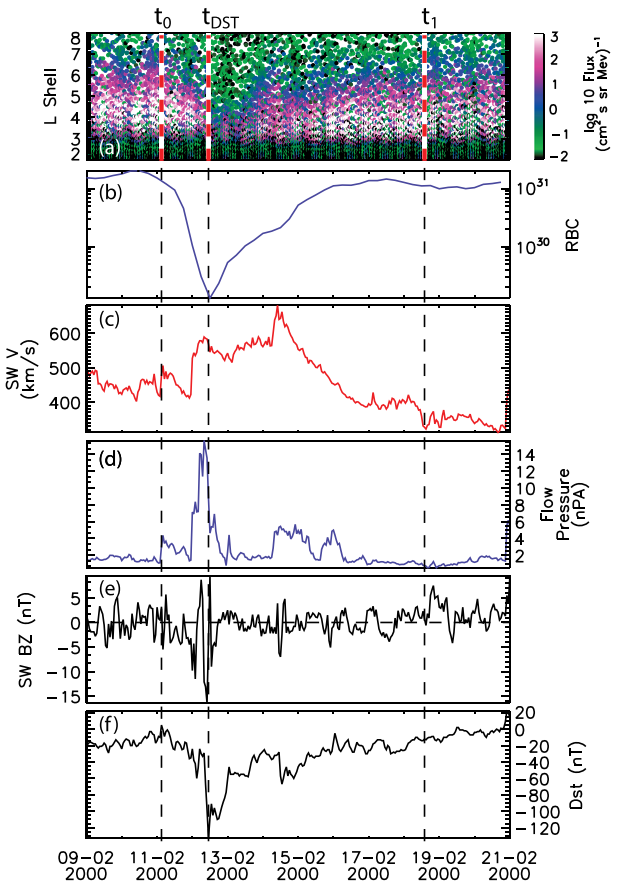

Figure 1. An example of a CME storm on 11 February 2000 and the identification of the start, minimum DST, and end of the storm, *t*0, *t*DST, and *t*1, respectively. (a) 1.5–6 MeV from SAMPEX, (b) 1.5–6 MEV RBC, (c) solar wind velocity, (d) solar wind dynamic pressure, (e) solar wind Bz, and (f) DSTst.

In our study we consider only storms where SAMPEX, OMNI, and ground-based magnetometer data are all available. Both OMNI and ground-based magnetometer data are used to derive parameters to characterize changes in RBC and thus are required for the subsequent analysis. We also remove duplicate and overlapping storms, as defined by the storm start and end times (see below). This leaves a total of 64 storms, 29 CME-driven storms, and 35 CIR-driven storms (see Supporting Information S3).

For each of the 64 storms we identify two distinct times: the start of the storm and the end of the storm determined by enhanced solar wind driving and storm time Dst in a similar manner to Murphy et al. (2018). Briefly, the start of each geomagnetic storm t_0 is identified by enhanced solar wind driving as the initial peak in solar wind dynamic pressure or solar wind velocity above nominally quiet time values of 500 km/s and 6 nPa (e.g., Hutchinson et al., 2011; Kataoka & Miyoshi, 2006). Similarly, the end of each storm is determined by either the recovery of Dst to nominally quiet values or the end of enhanced solar wind driving. The recovery of Dst is defined when Dst rises above −10 nT. If this threshold is never reached, then the recovery is defined as the final peak in Dst after which Dst is no longer increasing (recovering); that is, Dst reaches a steady state where it is no longer increasing, characterizing a quiet or near stable ring current following a recovery period. The end of enhanced solar driving is defined by the period when solar wind velocity or dynamic pressure drops below 450 km/s and 4 nPa for a period longer than 24 hr. The end of the storm is then defined as latest of these times, t_1. The solar wind and dynamic pressure thresholds to define the start and end of each storm have been identified by the superposed epoch studies of Kataoka and Miyoshi (2006) and Hutchinson et al. (2011). It is important to note that both the start and end times of the storms are defined independent of electron and RBC dynamics. Figure 1 shows an example CME storm, which occurred on 11 February 2000, and the identification of the start of the storm and end of the storm, t_0 and t_1 respectively. See figure caption for details. By identifying the start and the end of a storm, we investigate radiation belt electron dynamics, specifically net losses and net enhancements, throughout each phase with respect to potential drivers as described in the next section.

2.3. Storm Time Dynamics of the RBC Index

Figure 2 shows the variation RBC content during each CME-driven (top) and CIR-driven (bottom) geomagnetic storms. In order to plot the storms on a similar time axis, we have defined a common time during each storm as the time of minimum Dst $t_{\text{Dst.}}$ In the plots, t_{Dst} is set to zero. We then defined two intervals, the storm main phase, spanning from t_0–t_{Dst}, and the storm recovery phase, spanning from t_{Dst}–t_1. Since the storms can be of varying length and the duration of the main and recovery phases of each storm can be different, we have normalized the duration of each main phase to 24 hr (−24 to 0 hr) and each recovery phase to 120 hr (0–120 hr) such that each storm is on a similar time axis as was done in Hutchinson et al. (2011) (see also Halford et al., 2010; Yokoyama & Kamide, 1997). In Figure 2, each individual storm is plotted as a horizontal line at a constant *y* value, and the color denotes the variation in the RBC throughout the storm, normalized to 1 to aid intercomparison between storms. Finally, for each storm we mark the time of minimum RBC by a red circle. Evident in Figure 2 is that the time of minimum RBC (red circles) can be observed during either the storm main or recovery phases and is not clearly or systematically related to the time of minimum Dst. For CMEs the mean difference between the time minimum RBC compared to minimum Dst (in normalized time) is −0.27 hr with a standard deviation of 8.08 hr while CIRs have a mean and standard deviation of −1.75 and 10.32 hr, respectively. The minimum in RBC during geomagnetic storms naturally separates storms into two phases: one characterized by a net loss of radiation belt electrons where loss

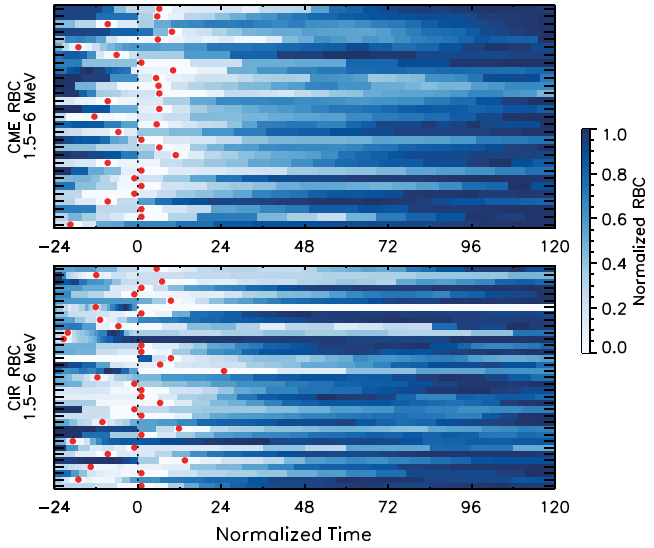

Figure 2. Variation in the normalized RBC during each of the CME-driven (top) and CIR-driven (bottom) storms. In each panel individual storms are plotted along the y axis along a normalized time axis. The zero time, t = 0, of each storm is the time of minimum Dst. The red dots show the time of minimum RBC during each storm.

processes dominate over acceleration processes and a second characterized by a net enhancement in radiation electrons where acceleration processes dominate over loss processes. The spread in the difference between the time of minimum Dst and minimum RBC, for both CME- and CIR-driven storms, demonstrates that though the time of minimum Dst may be a good way to separate the main and recovery phase for some aspects of storm analysis, such as ring current strength, it does not provide a clear separation of storm time radiation belt electron dynamics, which is the focus of this investigation here.

In this study we wish to investigate the processes driving periods of net electron loss and enhancement during storms as measured by RBC. For this reason, we use the time of minimum RBC t_{RBC} during each storm to define two intervals, an initial interval from the start of the storm to the time of minimum RBC, t_0–t_{RBC}, characterizing a period of net loss and a second interval from the time of minimum RBC to the end of the storm, t_{RBC}–t_1, characterizing a net enhancement in radiation belt electrons. In this way we can statistically investigate the physical processes during both radiation belt loss and acceleration during geomagnetic storms without the inherent pitfalls of a superposed epoch analysis, namely, smearing or averaging of temporal dynamics within a time series that occurs when the epoch time used for superposition is poorly related to the underlying dynamics of data set (cf. Figure 2).

In the remainder of this section we focus on analysis of the relative changes in RBC during t_0–t_{RBC} and t_{RBC}–t_1. Between t_0 and t_{RBC}, since we are focusing on how much of the belt is lost, we examine the fractional change in RBC as $_{RBC\ loss} = RBC(t_{RBC})/RBC(t_0)$, which is the amount of the radiation belt that is available to be lost during any particular storm. During the second phase of the storm, t_{RBC}–t_1, since we are interested in how much new radiation belt flux is generated from the minimum, we examine the absolute change in RBC as $_{RBC\ acc} = RBC(t_1) - RBC(t_{RBC})$. Further, the fractional loss and absolute change in RBC during the two phases t_0–t_{RBC} and t_{RBC}–t_1 allows for a direct comparison between changes in RBC during each storm studied.

Figure 3 shows a log-log comparison of the fractional loss in RBC between t_0–t_{RBC} and the absolute change in RBC t_{RBC}–t_1 for CME-driven (blue) and CIR-driven (red) storms. Evident in Figure 3 is that there is no direct relationship between the loss and acceleration phase of each individual storm. Storms with a significant amount of loss in the initial phase t_0–t_{RBC} are not necessarily associated with large enhancements during the second phase t_{RBC}–t_1. There is also no clear separation between loss and enhancements observed during CME- and CIR-driven storms. Quantitatively, we can compare the distributions of $_{RBC\ loss}$ and $\Delta_{RBC\ acc}$ for CME- and CIR-driven storms using the two-sided two-sample Kolmgorov-Smirnov (KS) statistic. The KS statistic can be used to assess whether two samples could be random draws from the same parent distribution (Press, 1992). By comparing the cumulative distribution of two data sets, the KS statistic defines the maximum distance D between the cumulative distributions. If D is greater than a critical value (e.g., O'Connor & Kleyner, 2012) or the significance level is small (Press, 1992), then it is likely that the two data sets are drawn from two distinct distributions. If D is smaller than a critical value or the significance level is large, then we cannot reject the null hypothesis that the two data sets come from a common distribution of values. Table 1 shows the value of D when comparing the distributions of $_{RBC\ loss}$ and $_{RBC\ acc}$ for CME- and CIR-driven storms. In both cases the value of D is smaller than the critical value of D at a 95% confidence level, and the significance level is greater than 0.05. Together, this means that we cannot reject the null hypothesis and suggests that it is likely that changes in RBC as

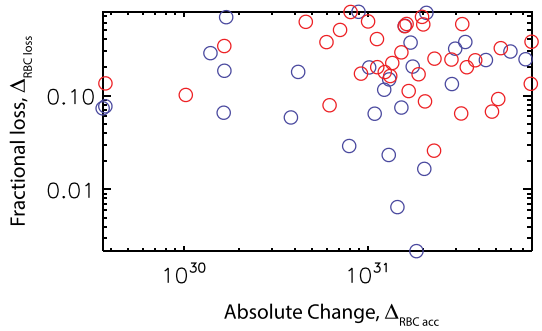

Figure 3. Comparison of the fractional change in RBC during net radiation belt losses and the absolute change in RBC during net enhancements. The distribution is divided into CME-driven (blue) and CIR-driven (red) storms for comparison.

Table 1
The Two-Sided Kolmgorov-Smirnov Statistic D for $_{RBC}$ and $|_{RBC}|$ During CME- and CIR-Driven Storms Compared to the Critical Value of D and Derived Significance Value

Storm phase	Derived value of D	Critical value of D at 95% confidence	Derived significance level	Are the variations in RBC during CME- and CIR-driven storms likely drawn from the same parent distribution?
t_0–t_{RBC}, $_{RBC}$	0.29	0.34	0.11	Yes
t_{RBC}–t_1, $\|_{RBC}\|$	0.19	0.34	0.56	Yes

measured by $_{RBC\ loss}$ and $_{RBC\ acc}$ for CME- and CIR-driven storms are drawn from similar distributions. This is a critical finding, as it suggests that the radiation belt responds in the same way during periods of net loss and enhancement, and independent of the large-scale storm driver and solar wind structure characterized as either a CIR or a CME. For the remainder of this section we consider changes in RBC driven by CME- and CIR-driven storms to be part of a similar distribution and compare these changes to known drivers of radiation belt electron loss, acceleration, and transport.

Utilizing the RBC index, we can analyze the $_{RBC\ loss}$ and $_{RBC\ acc}$ shown in Figure 3 to investigate the role of solar wind and magnetospheric activity and specific physical processes in driving periods of net loss and net enhancements, during geomagnetic storms. During net losses (t_0–t_{RBC}), we compare $_{RBC\ loss}$ to minimum magnetopause distance as a proxy for loss due to magnetopause shadowing (West et al., 1972) and minimum Sym-H as an estimate of ring current strength and outward adiabatic transfer leading to enhanced loss through the magnetopause. In both of these situations, radiation belt electron loss may result from the intersection of the last closed drift shell with the magnetopause boundary (e.g., Olifer et al., 2018). We also compare $_{RBC\ loss}$ with the duration of the loss phase, the summed geomagnetic index Kp, and total ULF wave power (as a proxy for ULF wave radial diffusion) during the loss period. For example, increased geomagnetic and ULF wave activity might be expected to lead to increased loss via enhance precipitation during the initial period of a storm (e.g., O'Brien et al., 2004) or outward radial diffusion following an initial period of magnetopause shadowing (e.g., Shprits et al., 2006).

During net enhancements in RBC (t_{RBC}–t_1), we compare $_{RBC\ acc}$ to total solar wind velocity and total solar wind energy input estimated by the sum of solar wind coupling function (ε parameter) (Perreault & Akasofu, 1978) over the acceleration phase, the duration of the acceleration phase, substorm activity and strength as estimated from the summed auroral electrojet index AE (which additionally may also be considered to be a proxy for VLF waves, e.g., Meredith et al., 2001), and the total ULF wave power. We hypothesize that increases in these parameters during the enhancement phase of storms can be expected to lead to increased acceleration and transport of relativistic electrons within the outer radiation belt.

Changes in the RBC during both periods of net loss and enhancements are compared to the total ULF wave power as a proxy for the strength of radial diffusion. During periods of net loss and net enhancements, we expect ULF wave power to be a proxy for electron loss through outward radial diffusion (e.g., Shprits et al., 2006; Turner et al., 2012a) and enhanced acceleration via either inward radial diffusion (e.g., Ma et al., 2018) or coherent ULF wave-particle interactions (e.g., Mann et al., 2013). Further, we assume that periods of net loss occur during a time interval when a negative gradient in electron phase space density existed in order to facilitate outward radial diffusion and periods of net enhancements occur during an interval when a positive gradient in electron phase space density existed to facilitate inward radial diffusion (e.g., Mann et al., 2016, supplementary material). The total ULF wave power is estimated from a database of hourly power spectra calculated from the east-west magnetic field component observed by ground-based magnetometers (Murphy et al., 2011; Pahud et al., 2009; Rae et al., 2012). Each hourly power spectrum is summed between 0.83 and 15.83 mHz, providing an estimate of ULF wave power. These hourly estimates are then summed over the duration of the loss or acceleration phase to provide estimates of the total ULF wave power during each phase. The east-west magnetic field component is used as it is expected to map to an azimuthal electric field (Ozeke et al., 2009), which can drive strong radial diffusion in the outer radiation belt (Ozeke et al., 2013). For the purpose of this study we use data from two ground-based magnetometer stations, Gillam (GILL) and Pinawa (PINA), both stations in the Canadian Array for Realtime

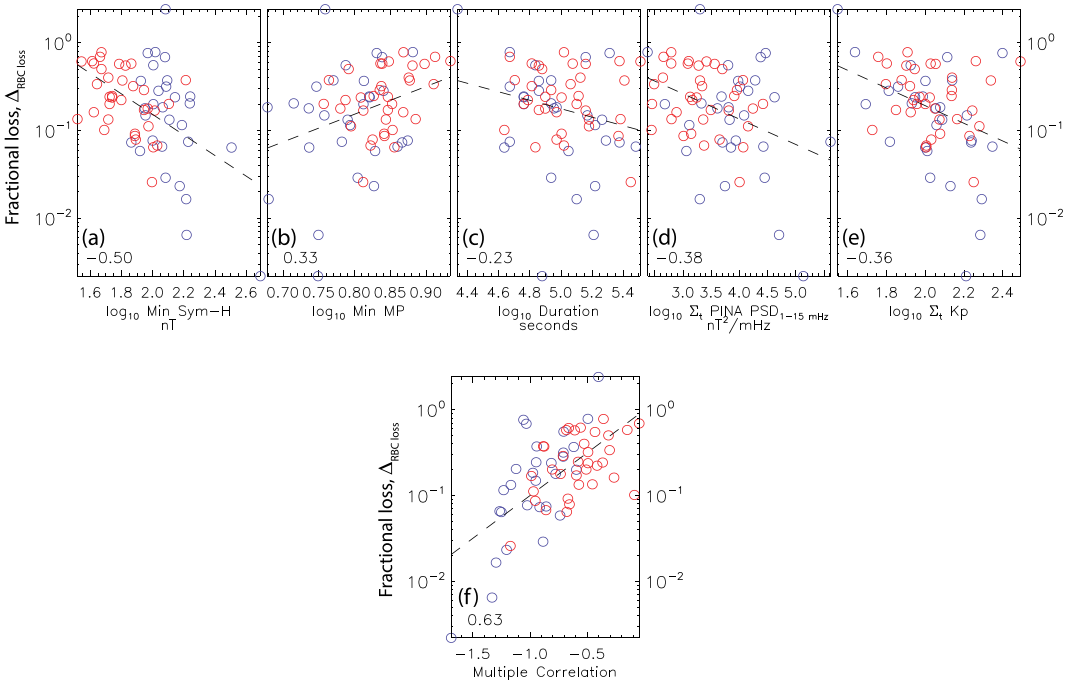

Figure 4. Log-log plot of the fractional change in RBC during storm time radiation belt losses during CME (blue) and CIR (red) storm as a function of (a) minimum SYM-H during the loss phase, (b) minimum magnetopause location during the loss phase, (c) loss phase duration, (d) total ULF wave power during the loss phase, and (e) total Kp. Panel (f) shows the multiple regression of minimum SYM-H (a), minimum magnetopause distance (b), loss phase duration (c), and total Kp (e) as a function of fractional change in RBC. The correlation coefficient is shown in the bottom left corner of each panel. The dashed lines show the linear regression of each distribution.

Investigations of Magnetic Activity (CARISMA) (Mann et al., 2008) magnetometer network, and for simplicity we consider only a single station during each storm phase.

Figure 4 shows the log-log comparison of the fractional change in RBC$_{RBC\ loss}$ between t_0–t_{RBC} for each storm as a function of (a) Sym-H, (b) minimum magnetopause distance, (c) loss phase duration, (d) total ULF wave power, and (e) summed Kp for all storms. In the bottom left of each panel, the correlation between the fractional loss and driver is shown for the entire distribution, and the dashed line shows the linear fit to each distribution. Evident in Figures 4a–4e is that when the magnetopause is closer to the Earth and during enhancements in geomagnetic activity, there is more loss in the radiation belt.

Since we expect that loss processes may act in unison during periods of strong net radiation belt loss, a multiple regression and correlation analysis can help to asses which processes are most important to net radiation belt loss during geomagnetic storms. For each combination of loss processes shown in Figures 4a–4e, that is, a total of 26 combinations, we perform a multiple linear regression fit with $\Delta_{RBC\ loss}$ in log space and determine the resulting correlation of the fit with $\Delta_{RBC\ loss}$. For example, considering minimum Sym-H and ULF wave power, we fit $\Delta_{RBC\ loss}$ to a function of the form

$$log_{10}(\Delta_{RBC}) = a_0 \times log_{10}(Sym - H_{min}) + a_1 \times log_{10}\left(\sum_t ULF_{\mathrm{PSD}}\right).$$

We then identify the fit where the correlation is maximized and where the coefficients of the fit make physical sense. Figure 4f shows this multiple regression analysis with the variables Sym-H, loss phase duration, minimum magnetopause distance, and summed Kp, with Δ_{RBC}. These four variables give the highest correlation in the multiple regression analysis and where the coefficients of the fit make physical sense. This is evidenced by the clear linear relationship.

Figure 5 shows a similar analysis as in Figure 4 but for the acceleration phase of each storm. The absolute change in RBC $\Delta_{RBC\ acc}$ is plotted against (a) solar wind energy input, (b) total solar wind velocity, (c)

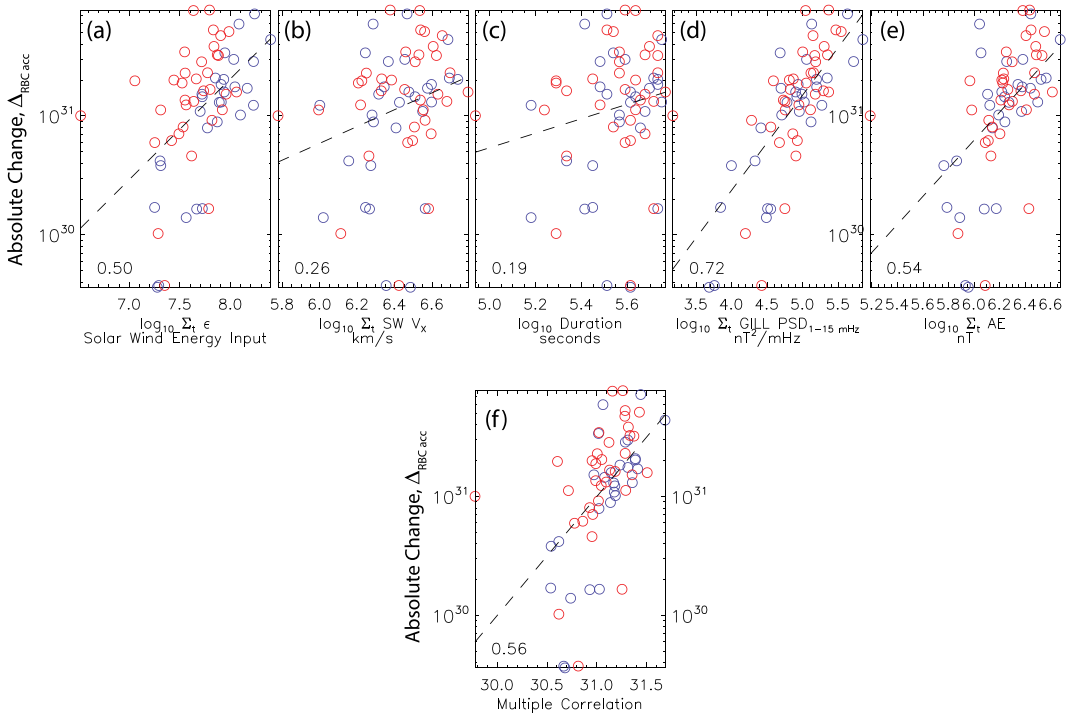

Figure 5. Log-log plot of the absolute change in RBC during storm time net RBC enhancements during CME (blue) and CIR (red) geomagnetic storms as a function of the following parameters linked to electron acceleration: (a) solar wind coupling function, (b) solar wind velocity, (c) acceleration phase duration, (d) total ULF wave power during the acceleration phase, and (e) total AE. Panel (f) shows the result from a multiple regression of solar wind energy input (a) and AE (b) with the absolute change in RBC during the acceleration phase. The correlation coefficient is shown in the bottom left of each panel. The dashed lines show the linear regression for each panel.

acceleration phase duration, (d) total ULF wave power from GILL, and (e) total AE, during the acceleration phase in the same format as Figure 4. Similar to the loss phase, enhanced solar wind energy input and increasingly intense geomagnetic activity during the acceleration phase lead to a larger enhancement in RBC during storms following periods of net loss. This is most clearly evident in Figure 5d where increased ULF wave power leads to a higher RBC.

We also perform the same multiple regression analysis for every combination of variables in Figures 5a–5e with net radiation belt enhancements $\Delta_{RBC\ acc}$. This is shown in Figure 5f. The correlation peaks, while maintaining coefficients that make physical sense, when using solar wind energy input and AE with a value of 0.56. When considering multiple variables, the correlation is lower than when considering ULF wave power alone.

The multiple regression and correlation analysis presented above has three caveats, which are important to note and which we discuss in detail below.

When investigating net losses and enhancements in the RBC in Figures 4 and 5 we use two magnetometer stations to estimate the strength of radial diffusion. During periods of net RBC losses, we use the low latitude Pinawa magnetometer station ($L \sim 4.06$) located near the center of the radiation belt to assess the connection between RBC and the ULF waves which might deplete the belts during outward radial diffusion along a negative phase space density gradient (Turner et al., 2012a). Since the radiation belt flux peaks in this region, for ULF waves to contribute significantly to losses seen in RBC arising from outward radial diffusion following an initial period of magnetopause shadowing requires ULF power to be significant there. During periods of net RBC enhancements, we use the higher-latitude Gillam magnetometer station ($L \sim 6.15$) near the outer edge of the outer radiation belt. As the radiation belt recovers due to the inward transport of available source electrons arising for instance from substorm injections (Baker et al., 1998; Boyd et al., 2016; Forsyth et al., 2016; Jaynes et al., 2015; Murphy et al., 2018), inward transport down a positive radial phase space

gradient can have an impact on RBC (Mann et al., 2016; Mann & Ozeke, 2016). To impact RBC, the newly supplied radiation belt electrons of course do not need to reach all the way the heart of the belt at $L \sim 4$ and will be expected to be seen in the RBC as soon as they are transported to the outer edge of the belt so long as their energy is high enough to add to the RBC count at those L-shells. Despite the use of different stations in the analysis reported here for the loss and acceleration phases, the results shown in Figures 4 and 5 are largely independent of the magnetometer station used in the analysis; this is likely because ULF wave power is in general correlated as function of L (Mathie & Mann, 2001).

Due to limited in situ coverage of the magnetosphere during the SAMPEX era, it is impossible to construct a continuous and global database of direct measurements of the processes controlling radiation belt dynamics, for example, VLF and EMIC wave power. For this reason, in the analysis presented above, we have chosen to use proxies, including AE, as estimates for these processes, as these proxies provide a continuous data set with which to complete the statistical analysis.

Finally, the multiple regression and correlation analysis shown in Figures 4f and 5f does not account for possible correlation between the input variables (multicollinearity). While this does not affect the multiple regressions ability to determine a good fit, it may lead to large standard errors in the estimate of fit coefficients, which poses problems when trying to physically interpret the coefficients (Osthus et al., 2014). Accounting for this multicollinearity can be difficult when considering solar wind driving and the response of the magnetosphere as the two systems are highly coupled, which naturally leads multicollinearity. Some attempt has been made to mitigate this by only considering fits which make physical sense and by limiting the number of input parameters to those which can be linked to specific drivers of electron dynamics. However, even in this case multicollinearity may lead to a biased estimate of the fit coefficients (Osthus et al., 2014, Appendix A). Future work expanding the analysis here should employ additional techniques to help mitigate the effects of multicollinearity (e.g., principle component analysis).

3. Discussion and Conclusions

Understanding the dominant processes driving electron loss and acceleration during geomagnetic storms is critical for space weather and radiation belt forecasting. In this manuscript we used data from the SAMPEX PET instrument to investigate the dynamics of the outer radiation belt during 29 CME-driven storms and 35 CIR-driven storms. In order to reduce the dimensionality of the data from SAMPEX and study the temporal dynamics of outer radiation belt electrons in a large number of events, we use a RBC index derived from observations of electron flux between fixed energies of 1.5–6 MeV and across an L-shell range from $L = 2$ to $L = 8$. The RBC index provides an estimate of the total number of electrons in the outer radiation belt and is ideal for statistical studies, as it reduces the dimensionality of the data set by removing the radial or L-shell dependence (Baker et al., 2004; Forsyth et al., 2016; Murphy et al., 2018).

Our analysis of the RBC index during CIR- and CME-driven geomagnetic storms highlights five key aspects of outer radiation belt electron dynamics.

1. First, the minimum in Dst does not coincide with the minimum of RBC. There can be 30–120 min offset between the two parameters.
2. Second, CME- and CIR-driven storms both show a period of net loss followed by a net enhancement of radiation belt electrons during geomagnetic storms. Analysis of changes in RBC demonstrate that intervals of net radiation belt loss and intervals of subsequent RBC enhancement during different storms are drawn from the same distribution, such that these dynamics are independent of the structure of the large-scale storm driver in the solar wind, that is, whether the storm resulted from either a CME or a CIR.
3. The net loss of electrons during geomagnetic storms is most strongly related to the minimum in Sym-H during the loss period, minimum magnetopause location, and duration of the loss period. All three of these parameters affect the amount of radiation belt electron loss observed.
4. The net enhancement of electrons during geomagnetic storms is most strongly related to the total ULF wave power during the enhancement period where the RBC index increases.
5. Both periods of net enhancements and net losses of radiation belt electrons during geomagnetic storms can be considered to act effectively independently as they have sufficiently different dependencies on physical drivers. By separating storms into periods of net radiation belt electron loss and enhancements, these periods can be separately investigated without conflating together intervals of electron loss and

enhancement thereby allowing for a more physically meaningful analysis of storm time radiation belt dynamics.

We discuss these points further below.

As shown in section 2 above, the time of minimum RBC during any given storm naturally divides a storm into two periods: an initial period that is dominated by electron loss and a second period dominated by electron enhancements, which is particularly useful when studying the large-scale drivers of radiation belt acceleration or loss, whatever those processes may be. As shown in Figure 2 this time can occur during either the storm main phase (preminimum Dst) or the storm recovery phase (postminimum Dst), such that neither phase consistently characterizes changes in storm time electron dynamics (e.g., Borovsky & Shprits, 2017). This is not surprising; while the Dst index may be an indicator of the strength of any particular geomagnetic storm and terrestrial ring current and provides insight into adiabatic changes in electron flux (e.g., H. Kim & Chan, 1997), it is also a measure of both the magnetopause currents (e.g., O'Brien & McPherron, 2000) and cross-tail current systems (Turner et al., 2000). If we wish to understand and statistically characterize storm time radiation belt electron dynamics, it is more meaningful to use the time of minimum RBC as opposed to the time of minimum Dst.

The results in Figure 3 demonstrate that both CME- and CIR-driven storms can experience large variations in electron loss and acceleration during any particular storm. There is also no clear separation between the distribution of losses and enhancements for CME- and CIR-driven storms as measured by the Kolmgorov-Smirnov statistic. This suggests that the changes in RBC are part of a single distribution as opposed to two different distributions dependent on CME or CIR storm drivers. This statistical analysis suggests that the strength of the physical processes determine the behavior of the outer radiation belt, not the exact nature of the solar wind driver that generates the physical response. In other words, the magnetosphere does not register whether the solar wind driver is a CIR or a CME; rather, it just responds to the efficiency of solar wind driving resulting from the structure the solar wind and response of the magnetosphere irrespective of whether it is categorized as a CME or CIR (e.g., Mathie & Mann, 2000; O'Brien et al., 2003, 2004; Shprits et al., 2013; Turner et al., 2012a; Ukhorskiy et al., 2010).

In Figure 4 we presented a log-log plot of the fractional change in RBC during the interval of net electron loss of each of the geomagnetic storms as a function of four geomagnetic variables indicative of storm strength and which have been linked with specific electron loss processes. Storms with larger Sym-H result in more radiation belt electron loss; there is also more loss during storms where the magnetopause is closer to the Earth as well as those which have enhanced ULF wave power; conversely, there is little relation between the duration of the loss phase and the overall amount of radiation belt electron loss. This suggests that the loss occurs rapidly or at least is not developed more slowly and cumulatively in response to the continuous and more gradual action of an ongoing but less efficient loss processes.

However, we do not expect individual loss mechanisms to act independently. Rather, loss processes are more likely to act additively to produce the observed overall net loss. Figure 4f shows support for this hypothesis in the form of the multiple regression analysis of the fractional loss as a function of Sym-H, minimum magnetopause distance, duration of the loss phase period, and summed Kp during the loss period. Using a combination of these four parameters provides the highest correlation between the fractional loss and geomagnetic variables, which may be related to storm time radiation belt loss.

In the context of previous work, the results shown in Figure 4 can also be used to assess the physical processes and the sequence of events associated with the observed loss. As a CME or CIR impacts the magnetosphere, the magnetopause typically moves inward due to enhanced southward IMF and increased solar wind dynamic pressure (e.g., Shue et al., 1998; Sibeck, 1990). The inward motion of the magnetopause results in magnetopause shadowing (West et al., 1972): storms where the magnetopause pushes closer to the Earth resulting in the largest loss. Strong geomagnetic activity coupled with magnetopause shadowing further aids in the loss of radiation belt electrons. Magnetopause shadowing creates a negative gradient in the electron phase space density allowing for additional loss driven by enhanced ULF wave power and outward radial diffusion (Loto'aniu et al., 2010; Mann et al., 2016; Shprits et al., 2006; Turner et al., 2012a). Enhancements in the ring current also push radiation belt electrons closer to the magnetopause aiding in

the loss of electrons through the magnetopause (e.g., Ukhorskiy et al., 2006). Finally, the duration of the loss period tends to generate a larger overall loss.

A similar analysis can be performed to determine how the outer radiation belt responds to multiple solar wind and geomagnetic drivers during the periods of net RBC enhancements during geomagnetic storms (cf. Figure 5). The analysis in Figure 5 demonstrates that net enhancements of RBC during the acceleration phase correlate remarkably well with total ULF wave power (Mathie & Mann, 2000). Both the Akasofu ε parameter and AE (Figures 5a and 5e), proxies for solar wind energy input, and substorm and VLF wave activity are also well correlated with increases in RBC. Solar wind velocity and the acceleration phase duration are both poorly correlated with net changes in RBC during the acceleration phase. Surprisingly, there is also a stronger relationship between intervals of radiation belt electron enhancements and ULF wave power alone than with any combination of variables in a multiple regression analysis.

Overall, the results shown in Figures 5 suggest that ULF waves (e.g., Brautigam & Albert, 2000; I.R. Mann et al., 2012; Mathie & Mann, 2000; O'Brien et al., 2003; Ozeke et al., 2013), substorm and VLF wave activity (as measured by AE) (e.g., Meredith et al., 2001, 2002), and solar wind driving (e.g., Baker et al., 1990; Lyatsky & Khazanov, 2008; Rigler, 2004; Rigler et al., 2007) play a role in the storm time enhancement of radiation belt electron content, consistent with previous work. As described in Jaynes et al. (2015), it is likely that substorms provide an enhanced source of lower energy seed electrons for subsequent acceleration to relativistic energies (Baker et al., 1998 e.g., Boyd et al., 2016). Strong VLF wave activity also driven by substorm activity (e.g., Li et al., 2014; Meredith et al., 2002), and intense ULF wave power (e.g., Mathie & Mann, 2000; O'Brien et al., 2003) and a positive phase space density gradient developing in the response to substorm activity (e.g., Murphy et al., 2018) lead to acceleration and increases in electron flux consistent with the correlations with net enhancement of the RBC index reported here.

Finally, our analysis of the net radiation belt loss and enhancements during geomagnetic storms demonstrates that the correlations of solar wind and geomagnetic parameters are different for the loss and acceleration phases. As a result, no single variable can be successfully used to parameterize the overall response of the outer radiation belt during geomagnetic storms. This provides a powerful explanation for the previously reported lack of correlation between prestorm and poststorm fluxes in the outer radiation belt (e.g., Anderson et al., 2015; Reeves et al., 2003). If the loss and acceleration phases have sufficiently different driver dependencies, then attempts to correlate prestorm and poststorm fluxes naturally generate such a conclusion. Thus, these two phases can be considered to act effectively independently. It is the superposition of the different solar wind and geomagnetic activity dependencies of these two phases that only when taken together can explain the overall response of the RBC during geomagnetic storms.

The results presented here provide clear support for a framework that can explain both losses and enhancements during geomagnetic storms and if exploited appropriately could lead to significant improvements in radiation belt forecasting. Future work expanding the concepts presented here could additionally utilize data from the Van Allen Probes to incorporate EMIC and VLF wave power as additional parameters into this framework. For example, recent work has demonstrated that EMIC wave occurrence peaks during the start of a storm (Halford et al., 2010) and may be important in radiation belt loss (e.g., Shprits et al., 2013). Direct observations of VLF wave power will also likely be better than inferring wave activity from proxies such as the AE index (Watt et al., 2017). Similarly, the use of electron phase space density as opposed to flux in deriving a RBC index might further improve the inferred correlations. With regard to modeling and forecasting the radiation belt during geomagnetic storms, using the framework presented here and separating periods of net loss and enhancements may provide more meaningful and hopefully more accurate basis for simulations. For example, separating periods of net loss from net enhancement may reduce errors propagated through models that are unable to fully capture the dynamics of either process. This in turn would provide more meaningful comparisons to data that could potentially be translated into more accurate forecast frameworks.

Acknowledgments
K. R. M is supported by an NSERC Postdoctoral Fellowship, NSF Grant 1602403, and NASA Grants 18-HGIO18_2-0122 and 18-HSWO2R18-0010. I. R. M. is supported by a Discovery Grant from Canadian NSERC. D. G. S is supported by the NASA Van Allen Probes Mission. I. J. R. is funded in part by the UK Science and Technology Facilities Council (STFC) Grants ST/L000563/1 and ST/N000722 and the UK Natural Environment Research Council (NERC) Grant NE/L007495/1. C. E. J. W. is funded in part by the UK STFC Grant ST/M000885/1 and NERC Grant NE/P017274/1. The Canadian Array for Real-time Investigations of Magnetic Activity (CARISMA; www.carisma.ca) is operated by the University of Alberta, funded by the Canadian Space Agency. SAMPEX data are provided through CDAweb (cdaweb.gsfc.nasa.gov), and solar wind and geomagnetic indices are provided through OMNIweb (omniweb.gsfc.nasa.gov). The RBC index used in this investigation as well as a list of storms studied can be found on the Digital Repository at the University of Maryland (at https://doi.org/10.13016/jew4-fjgm). The repository contains a detailed description of the data set and list of storms, which is also described in the supporting information.

References

Anderson, B. R., Millan, R. M., Reeves, G. D., & Friedel, R. H. W. (2015). Acceleration and loss of relativistic electrons during small geomagnetic storms. *Geophysical Research Letters*, *42*, 10,113–10,119. https://doi.org/10.1002/2015GL066376

Baker, D., Li, X., Blake, J., & Kanekal, S. (1998). Strong electron acceleration in the Earth's magnetosphere. *Advances in Space Research*, *21*(4), 609–613. https://doi.org/10.1016/S0273-1177(97)00970-8

Baker, D. N., & Blake, J. B. (2012). SAMPEX: A long-serving radiation belt sentinel. *Geophysical Monograph Series*, *199*, 21–40. https://doi.org/10.1029/2012GM001368

Baker, D. N., Kanekal, S. G., & Blake, J. B. (2004). Characterizing the Earth's outer Van Allen zone using a radiation belt content index. *Space Weather*, *2*, n/a–n/a. https://doi.org/10.1029/2003SW000026

Baker, D. N., McPherron, R. L., Cayton, T. E., & Klebesadel, R. W. (1990). Linear prediction filter analysis of relativistic electron properties at 6.6 RE. *Journal of Geophysical Research*, *95*(A9), 15,133–15,140. https://doi.org/10.1029/JA095iA09p15133

Bingham, S. T., Mouikis, C. G., Kistler, L. M., Boyd, A. J., Paulson, K., Farrugia, C. J., et al. (2018). The outer radiation belt response to the storm time development of seed electrons and chorus wave activity during CME and CIR storms. *Journal of Geophysical Research: Space Physics*, (123), 10–39 2018JA025963. https://doi.org/10.1029/2018JA025963

Borovsky, J. E. (2014). Canonical correlation analysis of the combined solar wind and geomagnetic index data sets. *Journal of Geophysical Research: Space Physics*, *119*, 5364–5381. https://doi.org/10.1002/2013JA019607

Borovsky, J. E., & Shprits, Y. Y. (2017). Is the Dst index sufficient to define all Geospace storms? *Journal of Geophysical Research: Space Physics*, *122*, 11,543–11,547. https://doi.org/10.1002/2017JA024679

Boyd, A. J., Spence, H. E., Huang, C. L., Reeves, G. D., Baker, D. N., Turner, D. L., et al. (2016). Statistical properties of the radiation belt seed population. *Journal of Geophysical Research, A: Space Physics*, *121*, 7636–7646. https://doi.org/10.1002/2016JA022652

Brautigam, D. H., & Albert, J. M. (2000). Radial diffusion analysis of outer radiation belt electrons during the October 9, 1990, magnetic storm. *Journal of Geophysical Research: Space Physics*, *105*, 291–309. https://doi.org/10.1029/1999JA900344

Chen, Y., Reeves, G. D., Cunningham, G. S., Redmon, R. J., & Henderson, M. G. (2016). Forecasting and remote sensing outer belt relativistic electrons from low earth orbit. *Geophysical Research Letters*, *43*, 1031–1038. https://doi.org/10.1002/2015GL067481

Denton, M. H., Borovsky, J. E., Skoug, R. M., Thomsen, M. F., Lavraud, B., Henderson, M. G., et al. (2006). Geomagnetic storms driven by ICME- and CIR-dominated solar wind. *Journal of Geophysical Research: Space Physics*, *111*, 1–12. https://doi.org/10.1029/2005JA011436

Forsyth, C., Rae, I. J., Murphy, K. R., Freeman, M. P., Huang, C. L., Spence, H. E., et al. (2016). What effect do substorms have on the content of the radiation belts? *Journal of Geophysical Research: Space Physics*, *121*(7), 6292–6306. https://doi.org/10.1002/2016JA022620

Halford, A. J., Fraser, B. J., & Morley, S. K. (2010). EMIC wave activity during geomagnetic storm and nonstorm periods. *CRRES results*, *115*(May), 1–15. https://doi.org/10.1029/2010JA015716

Hietala, H., Kilpua, E. K. J., Turner, D. L., & Angelopoulos, V. (2014). Depleting effects of ICME-driven sheath regions on the outer electron radiation belt. *Geophysical Research Letters*, *41*, 2258–2265. https://doi.org/10.1002/2014GL059551

Horne, R. B., Glauert, S. A., Meredith, N. P., Koskinen, H. E. J., Vainio, R., Afanasiev, A., et al. (2013). Forecasting the Earth's radiation belts and modelling solar energetic particle events: Recent results from SPACECAST. *Journal of Space Weather and Space Climate*, *3*, A20–A20. https://doi.org/10.1051/swsc/2013042

Hutchinson, J. A., Wright, D. M., & Milan, S. E. (2011). Geomagnetic storms over the last solar cycle: A superposed epoch analysis. *Journal of Geophysical Research: Space Physics*, *116*, n/a–n/a. https://doi.org/10.1029/2011JA016463

Jaynes, A. N., Baker, D. N., Singer, H. J., Rodriguez, J. V., Loto'aniu, T. M., Ali, A. F., et al. (2015). Source and seed populations for relativistic electrons: Their roles in radiation belt changes. *Journal of Geophysical Research: Space Physics*, *120*, 7240–7254. https://doi.org/10.1002/2015JA021234

Kanekal, S. G., Baker, D. N., & Blake, J. B. (2001). Multisatellite measurements of relativistic electrons: Global coherence. *Journal of Geophysical Research: Space Physics*, *106*, 29,721–29,732. https://doi.org/10.1029/2001JA000070

Kanekal, S. G., Baker, D. N., Fennell, J. F., Jones, A., Schiller, Q., Richardson, I. G., et al. (2016). Prompt acceleration of magnetospheric electrons to ultrarelativistic energies by the 17 march 2015 interplanetary shock. *Journal of Geophysical Research: Space Physics*, *121*, 7622–7635. https://doi.org/10.1002/2016JA022596

Kataoka, R., & Miyoshi, Y. (2006). Flux enhancement of radiation belt electrons during geomagnetic storms driven by coronal mass ejections and corotating interaction regions. *Space Weather*, *4*, 1–11. https://doi.org/10.1029/2005SW000211

Kilpua, E. K. J., Hietala, H., Turner, D. L., Koskinen, H. E. J., Pulkkinen, T. I., Rodriguez, J. V., et al. (2015). Unraveling the drivers of the storm-time radiation belt response. *Geophysical Research Letters*, (May), n/a-n/a, *42*, 3076–3084. https://doi.org/10.1002/2015GL063542

Kim, H., & Chan, A. A. (1997). Fully adiabatic changes in storm time relativistic electron fluxes. *Journal of Geophysical Research*, *102*(A10), 22107–22116. https://doi.org/10.1029/97JA01814

Kim, K. C., Lee, D.-Y., Kim, H.-J., Lee, E. S., & Choi, C. R. (2010). Numerical estimates of drift loss and Dst effect for outer radiation belt relativistic electrons with arbitrary pitch angle. *Journal of Geophysical Research*, *115*, A03208. https://doi.org/10.1029/2009JA014523

Li, W., Shprits, Y. Y., & Thorne, R. M. (2007). Dynamic evolution of energetic outer zone electrons due to wave-particle interactions during storms. *Journal of Geophysical Research*, *112*, 1–13. https://doi.org/10.1029/2007JA012368

Li, W., Thorne, R. M., Ma, Q., Ni, B., Bortnik, J., Baker, D. N., et al. (2014). Radiation belt electron acceleration by chorus waves during the 17 March 2013 storm. *Journal of Geophysical Research: Space Physics*, *119*, 4681–4693. https://doi.org/10.1002/2014JA019945

Loto'aniu, T. M., Singer, H. J., Waters, C. L., Angelopoulos, V., Mann, I. R., Elkington, S. R., & Bonnell, J. W. (2010). Relativistic electron loss due to ultralow frequency waves and enhanced outward radial diffusion. *Journal of Geophysical Research: Space Physics*, *115*, 1–13. https://doi.org/10.1029/2010JA015755

Lyatsky, W., & Khazanov, G. V. (2008). A predictive model for relativistic electrons at geostationary orbit. *Geophysical Research Letters*, *35*, 1–5. https://doi.org/10.1029/2008GL034688

Ma, Q., Li, W., Bortnik, J., Thorne, R. M., Chu, X., Ozeke, L. G., et al. (2018). Quantitative evaluation of radial diffusion and local acceleration processes during GEM challenge events. *Journal of Geophysical Research: Space Physics*, *123*, 1–15. https://doi.org/10.1002/2017JA025114

Mann, I. R., Milling, D. K., Rae, I. J., Ozeke, L. G., Kale, A., Kale, Z. C., et al. (2008). The upgraded CARISMA magnetometer array in the THEMIS era. *Space Science Reviews*, *141*(1–4), 413–451. https://doi.org/10.1007/s11214-008-9457-6

Mann, I. R., Murphy, K. R., Ozeke, L. G., Rae, I. J., Milling, D. K., & Kale, A. (2012). The role of ultralow frequency waves in radiation belt dynamics. *Geophysical Monograph Series*, *199*, 69–91. https://doi.org/10.1029/2012GM001349

Mann, I. R., Ozeke, L. G., Murphy, K. R., Claudepierre, S. G., Turner, D. L., Baker, D. N., et al. (2016). Explaining the dynamics of the ultra-relativistic third Van Allen radiation belt. *Nature Physics*, *12*(June), 1–6. https://doi.org/10.1038/nphys3799

Mann, I. R., Lee, E. A., Claudepierre, S. G., Fennell, J. F., Degeling, A., Rae, I. J., et al. (2013). Discovery of the action of a geophysical synchrotron in the Earth's Van Allen radiation belts. *Nature Communications*, *4*(1), 1–6. https://doi.org/10.1038/ncomms3795

Mann, I. R., & Ozeke, L. G. (2016). How quickly, how deeply, and how strongly can dynamical outer boundary conditions impact Van Allen radiation belt morphology? *Journal of Geophysical Research, A: Space Physics*, *121*(6), 5553–5558. https://doi.org/10.1002/2016JA022647

Mathie, R. A., & Mann, I. R. (2000). A correlation between extended intervals of Ulf wave power and storm-time geosynchronous relativistic electron flux enhancements. *Geophysical Research Letters*, *27*(20), 3261–3264. https://doi.org/10.1029/2000GL003822

Mathie, R. A., & Mann, I. R. (2001). On the solar wind control of Pc5 ULF pulsation power at mid-latitudes: Implications for MeV electron acceleration in the outer radiation belt. *Journal of Geophysical Research*, *106*(A12), 29,783–29,796. https://doi.org/10.1029/2001JA000002

Meredith, N. P., Horne, R. B., Anderson, R. R., & Horne, B. (2001). Substorm dependence of chorus amplitudes: Implications for the acceleration of electrons to relativistic energies. *Journal of Geophysical Research*, *106*(A7), 13,165–13,178. https://doi.org/10.1029/2000JA900156

Meredith, N. P., Horne, R. B., Iles, R. H. A., Thorne, R. M., Heynderickx, D., & Anderson, R. R. (2002). Outer zone relativistic electron acceleration associated with substorm-enhanced whistler mode chorus. *Journal of Geophysical Research*, *107*(A7). https://doi.org/10.1029/2001JA900146

Meredith, N. P., Thorne, R. M., Horne, R. B., Summers, D., Fraser, B. J., & Anderson, R. R. (2003). Statistical analysis of relativistic electron energies for cyclotron resonance with EMIC waves observed on CRRES. *Journal of Geophysical Research: Space Physics*, *108*(A6), 1–14. https://doi.org/10.1029/2002JA009700

Miyoshi, Y., & Kataoka, R. (2005). Ring current ions and radiation belt electrons during geomagnetic storms driven by coronal mass ejections and corotating interaction regions. *Geophysical Research Letters*, *32*, 1–5. https://doi.org/10.1029/2005GL024590

Miyoshi, Y., Kataoka, R., Kasahara, Y., Kumamoto, A., Nagai, T., & Thomsen, M. F. (2013). High-speed solar wind with southward interplanetary magnetic field causes relativistic electron flux enhancement of the outer radiation belt via enhanced condition of whistler waves. *Geophysical Research Letters*, *40*, 4520–4525. https://doi.org/10.1002/grl.50916

Morley, S. K., Friedel, R. H. W., Spanswick, E. L., Reeves, G. D., Steinberg, J. T., Koller, J., et al. (2010). Dropouts of the outer electron radiation belt in response to solar wind stream interfaces: Global positioning system observations. *Proceedings of the Royal Society A: Mathematical, Physical and Engineering Sciences*, *466*(2123), 3329–3350. https://doi.org/10.1098/rspa.2010.0078

Murphy, K. R., Watt, C. E. J., Mann, I. R., Jonathan Rae, I., Sibeck, D. G., Boyd, A. J., et al. (2018). The global statistical response of the outer radiation belt during geomagnetic storms. *Geophysical Research Letters*, *45*, 3783–3792. https://doi.org/10.1002/2017GL076674

Murphy, K. R., Mann, I. R., Jonathan Rae, I., & Milling, D. K. (2011). Dependence of ground-based Pc5 ULF wave power on F10.7 solar radio flux and solar cycle phase. *Journal of Atmospheric and Solar-Terrestrial Physics*, *73*(11–12), 1500–1510. https://doi.org/10.1016/j.jastp.2011.02.018

O'Brien, T. P., Looper, M. D., & Blake, J. B. (2004). Quantification of relativistic electron microburst losses during the GEM storms. *Geophysical Research Letters*, *31*, L04802. https://doi.org/10.1029/2003GL018621

O'Brien, T. P., Lorentzen, K. R., Mann, I. R., Meredith, N. P., Blake, J. B., Fennell, J. F., et al. (2003). Energization of relativistic electrons in the presence of ULF power and MeV microbursts: Evidence for dual ULF and VLF acceleration. *Journal of Geophysical Research: Space Physics*, *108*. https://doi.org/10.1029/2002JA009784

O'Brien, T. P., & McPherron, R. L. (2000). Forecasting the ring current index Dst in real time. *Journal of Atmospheric and Solar-Terrestrial Physics*, *62*(14), 1295–1299. https://doi.org/10.1016/S1364-6826(00)00072-9

O'Brien, T. P., McPherron, R. L., Sornette, D., Reeves, G. D., Friedel, R., & Singer, H. J. (2001). Which magnetic storms produce relativistic electrons at geosynchronous orbit? *Journal of Geophysical Research*, *106*(A8), 15,533–15,544. https://doi.org/10.1029/2001JA000052

O'Connor, P. D. T., & Kleyner, A. (2012). *Practical Reliability Engineering*. John Wiley.

Olifer, L., Mann, I. R., Morley, S. K., Ozeke, L. G., & Choi, D. (2018). On the role of last closed drift Shell dynamics in driving fast losses and Van Allen Radiation Belt extinction. *Journal of Geophysical Research: Space Physics*, *123*(5), 3692–3703. https://doi.org/10.1029/2018JA025190

Osthus, D., Caragea, P. C., Higdon, D., Morley, S. K., Reeves, G. D., & Weaver, B. P. (2014). Dynamic linear models for forecasting of radiation belt electrons and limitations on physical interpretation of predictive models. *Space Weather*, *12*, 426–446. https://doi.org/10.1002/2014SW001057

Ozeke, L. G., Mann, I. R., Murphy, K. R., Rae, I. J., & Chan, A. A. (2013). ULF wave-driven radial diffusion simulations of the outer radiation belt. *In Geophysical Monograph Series*, *199*, 139–150. https://doi.org/10.1029/2012GM001332

Ozeke, L. G., Mann, I. R., & Rae, I. J. (2009). Mapping guided Alfvén wave magnetic field amplitudes observed on the ground to equatorial electric field amplitudes in space. *Journal of Geophysical Research*, *114*, A01214. https://doi.org/10.1029/2008JA013041

Pahud, D. M., Rae, I. J., Mann, I. R., Murphy, K. R., & Amalraj, V. (2009). Ground-based Pc5 ULF wave power: Solar wind speed and MLT dependence. *Journal of Atmospheric and Solar-Terrestrial Physics*, *71*(10–11), 1082–1092. https://doi.org/10.1016/j.jastp.2008.12.004

Perreault, P., & Akasofu, S.-I. (1978). A study of geomagnetic storms. *Geophysical Journal International*, *54*(3), 547–573. https://doi.org/10.1111/j.1365-246X.1978.tb05494.x

Press, W. H. (1992). *Numerical recipes in C: The art of scientific computing*. New York: Cambridge Univ. Press.

Rae, I. J., Mann, I. R., Murphy, K. R., Ozeke, L. G., Milling, D. K., Chan, A. A., et al. (2012). Ground-based magnetometer determination of in situ Pc4-5 ULF electric field wave spectra as a function of solar wind speed. *Journal of Geophysical Research: Space Physics*, *117*, 1–17. https://doi.org/10.1029/2011JA017335

Reeves, G. D., McAdams, K. L., Friedel, R. H. W., & O'Brien, T. P. (2003). Acceleration and loss of relativistic electrons during geomagnetic storms. *Geophysical Research Letters*, *30*(10). https://doi.org/10.1029/2002GL016513

Reeves, G. D., Spence, H. E., Henderson, M. G., Morley, S. K., Friedel, R. H. W., Funsten, H. O., et al. (2013). Electron acceleration in the heart of the Van Allen radiation belts. *Science*, *341*(August), 991–994.

Rigler, E. J. (2004). Adaptive linear prediction of radiation belt electrons using the Kalman filter. *Space Weather*, *2*(3), 1–9. https://doi.org/10.1029/2003SW000036

Rigler, E. J., Wiltberger, M., & Baker, D. N. (2007). Radiation belt electrons respond to multiple solar wind inputs. *Journal of Geophysical Research: Space Physics*, *112*, 1–17. https://doi.org/10.1029/2006JA012181

Schrijver, C. J., Kauristie, K., Aylward, A. D., Denardini, C. M., Gibson, S. E., Glover, A., et al. (2015). Understanding space weather to shield society: A global road map for 2015–2025 commissioned by COSPAR and ILWS. *Advances in Space Research*, *55*(12), 2745–2807. https://doi.org/10.1016/j.asr.2015.03.023

Selesnick, R. S. (2006). Source and loss rates of radiation belt relativistic electrons during magnetic storms. *Journal of Geophysical Research: Space Physics*, *111*, A04210. https://doi.org/10.1029/2005JA011473

Selesnick, R. S., & Kanekal, S. G. (2009). Variability of the total radiation belt electron content. *Journal of Geophysical Research: Space Physics*, *114*, 1–10. https://doi.org/10.1029/2008JA013432

Shprits, Y. Y., Subbotin, D., Drozdov, A., Usanova, M. E., Kellerman, A., Orlova, K., et al. (2013). Unusual stable trapping of the ultrarelativistic electrons in the Van Allen radiation belts. *Nature Physics*, *9*(11), 699–703. https://doi.org/10.1038/nphys2760

Shprits, Y. Y., Thorne, R. M., Friedel, R., Reeves, G. D., Fennell, J., Baker, D. N., & Kanekal, S. G. (2006). Outward radial diffusion driven by losses at magnetopause. *Journal of Geophysical Research*, *111*, A11214. https://doi.org/10.1029/2006JA011657

Shue, J.-H., Song, P., Russell, C. T., Steinberg, J. T., Chao, J. K., Zastenker, G., et al. (1998). Magnetopause location under extreme solar wind conditions. *Journal of Geophysical Research*, *103*(A8), 17,691–17,700. https://doi.org/10.1029/98JA01103

Shumway, H., & Stoffer, D. (2006). Time series analysis and its applications. In *Time Series Analysis and Its Applications*. Springer New York: Springer. https://doi.org/10.1007/0-387-36276-2

Sibeck, D. G. (1990). A model for the transient magnetospheric response to sudden solar wind dynamic pressure variations. *Journal of Geophysical Research*, *95*, 3755–3771. https://doi.org/10.1029/JA095iA04p03755

Su, Z., Zhu, H., Xiao, F., Zong, Q.-G., Zhou, X.-Z., Zheng, H., et al. (2015). Ultra-low-frequency wave-driven diffusion of radiation belt relativistic electrons. *Nature Communications*, *6*(1), 10,096–10,098. https://doi.org/10.1038/ncomms10096

Tu, W., Cunningham, G. S., Chen, Y., Morley, S. K., Reeves, G. D., Blake, J. B., et al. (2014). Event-specific chorus wave and electron seed population models in DREAM3D using the Van Allen probes. *Geophysical Research Letters*, *41*, 1359–1366. https://doi.org/10.1002/2013GL058819

Tu, W., & Li, X. (2011). Adiabatic effects on radiation belt electrons at low altitude. *Journal of Geophysical Research: Space Physics*, *116*, 2–11. https://doi.org/10.1029/2011JA016468

Turner, D. L., Morley, S. K., Miyoshi, Y., Ni, B., & Huang, C. L. (2012b). Outer radiation belt flux dropouts: Current understanding and unresolved questions. *Geophysical Monograph Series*, *199*, 195–212. https://doi.org/10.1029/2012GM001310

Turner, D. L., O'Brien, T. P., Fennell, J. F., Claudepierre, S. G., Blake, J. B., Kilpua, E. K. J., & Hietala, H. (2015). The effects of geomagnetic storms on electrons in Earth's radiation belts. *Geophysical Research Letters*, *42*(21), 9176–9184. https://doi.org/10.1002/2015GL064747

Turner, D. L., Shprits, Y., Hartinger, M., & Angelopoulos, V. (2012a). Explaining sudden losses of outer radiation belt electrons during geomagnetic storms. *Nature Physics*, *8*(3), 208–212. https://doi.org/10.1038/nphys2185

Turner, N. E., Baker, D. N., Pulkkinen, T. I., & McPherron, R. L. (2000). Evaluation of the tail current contribution to Dst. *Journal of Geophysical Research*, *105*(A3), 5431–5439. https://doi.org/10.1029/1999JA000248

Ukhorskiy, A. Y., Anderson, B. J., Brandt, P. C., & Tsyganenko, N. A. (2006). Storm time evolution of the outer radiation belt: Transport and losses. *Journal of Geophysical Research*, *111*, 1–9. https://doi.org/10.1029/2006JA011690

Ukhorskiy, A. Y., Shprits, Y. Y., Anderson, B. J., Takahashi, K., & Thorne, R. M. (2010). Rapid scattering of radiation belt electrons by storm-time EMIC waves. *Geophysical Research Letters*, *37*(9), 1–5. https://doi.org/10.1029/2010GL042906

Watt, C. E. J., Rae, I. J., Murphy, K. R., Anekallu, C., Bentley, S. N., & Forsyth, C. (2017). The parameterization of wave-particle interactions in the outer radiation belt. *Journal of Geophysical Research*, *122*, 9545–9551. https://doi.org/10.1002/2017JA024339

West, H. I., Buck, R. M., & Walton, J. R. (1972). Shadowing of Electron azimuthal-drift motions near the noon magnetopause. *Nature Physical Science*, *240*(97), 6–7. https://doi.org/10.1038/physci240006a0

Yokoyama, N., & Kamide, Y. (1997). Statistical nature of geomagnetic storms. *Journal of Geophysical Research*, *102*(A7), 14,215–14,222. https://doi.org/10.1029/97JA00903

Yuan, C. J., & Zong, Q. G. (2012). Quantitative aspects of variations of 1.5-6.0 MeV electrons in the outer radiation belt during magnetic storms. *Journal of Geophysical Research: Space Physics*, *117*, 1–13. https://doi.org/10.1029/2011JA017346